Supporting Information for "Formation of ridges in a stable lithosphere in mantle convection models with a visco-plastic rheology"

A. Rozel[1], G. J. Golabek[1,2], R. Näf[1], P. J. Tackley[1]

Contents of this file

1. Text S1: Mapping the ridge only regime in cartesian geometry
2. Text S2: Surface fields
3. Text S3: Strain-rate fields

Corresponding author: A. Rozel, Institute of Geophysics, Department of Earth Sciences, ETH Zurich, Sonneggstrasse 5, 8092 Zurich, Switzerland. (antoinerozel@gmail.com)

[1]Institute of Geophysics, Department of Earth Sciences, ETH Zurich, Sonneggstrasse 5, 8092 Zurich, Switzerland.
(antoinerozel@gmail.com)

[2]Bayerisches Geoinstitut, University of Bayreuth, Universitätsstrasse 30, 95440 Bayreuth, Germany.

4. Text S4: Stationarity of the RO regime

5. Figure S1: Maps of convection regimes in cartesian geometry

6. Figure S2: Surface fields

7. Figure S3: Strain-rate fields

8. Figure S4: Initial temperature field

Additional Supporting Information (Files uploaded separately)

1. Caption for Table S1

2. Caption for Movie S1

Introduction

This supporting information file provides a discussion of the regimes obtained in cartesian geometry (see text S1), as shown in figure S1. Surface fields are displayed in Fig. S2 and discussed in text S2. The strain-rate fields corresponding to Fig. 1 are shown in Fig. S3 and discussed in text S3. Text S4 discusses in detail the generation and stationarity of the RO regime, which might depend on the initial temperature field depicted in Fig. S4. We also provide the caption for a table presenting the convection regimes obtained in all simulations (see table S1). Finally, a movie displaying alternating ridges, appearing at different sites while the convection mode changes, is discussed in section Movie S1.

Text S1: Mapping the ridge only regime in cartesian geometry

A preliminary set of simulations was performed in cartesian geometry employing an aspect ratio of 8:1 with periodic boundary conditions. The resolution in these models was 512 x 64 grid points. In these experiments, the rheology used was slightly different than

what we present in the main article. In this supporting material, the viscosity was defined as:

$$\eta = \eta_{ref} \exp\left(\frac{41.4465}{1+T} - \frac{41.4465}{2} + Vz'\right), \quad (1)$$

where z' is the dimensionless depth. This formulation is know as the Frank-Kamenetzkii approximation for the depth-dependent part of the viscosity. The temperature-dependent part is identical to the original definition used in the main article. All other parameters are identical to those applied in the main article and in the supporting information.

Fig. 1 shows the convection regimes obtained in this additional set of simulations applying 2D cartesian geometry. For sake of comparison, we superimpose in gray the data points and boundaries as obtained in 2D spherical annulus geometry (displayed in Figure 3 of the main article). In both subplots, the stagnant lid regime is represented by light blue color, the mobile lid regime is marked white, the episodic regime is represented by orange (using fading colors for the boundary with mobile lid regime since it is not precisely mapped out) and finally the RO regime is shown in purple. Cartesian simulations are represented by black squares, filled with green for the cases displaying the RO regime, or with red filling for the episodic regime.

The top panel of Fig. 1 shows that the RO regime can be present only for non-zero vertical viscosity contrasts. For cases in which $V = 0$, the episodic regime occurs for a considerable range of parameters, always being present between the mobile and stagnant lid regimes. The RO regime area is shifted upwards to larger viscosity contrasts compared

to what was obtained in spherical annulus geometry. The RO regime is found in the same friction coefficient range for both spherical annulus and cartesian geometries.

The bottom panel of Fig. 1 shows that even in cartesian geometry the RO regime can only be found in simulations in which a vertical viscosity contrast of at least 10^2 is imposed. The RO regime region is found at a similar location in the parameter space, although only cases considering friction coefficients greater than 0.18 lead to a stable ridge only state. Moreover, the episodic regime was observed at the junction between mobile, stagnant and RO areas in the parameter space. This result shows that the episodic regime is more likely to appear in cartesian geometry, which is consistent with what has been reported by *Moresi and Solomatov* [1998]; *Stein et al.* [2004]. *Foley and Becker* [2009] found the episodic regime between mobile and stagnant lid regimes in 3D spherical geometries, using homogeneous yield stresses through the entire lithosphere.

Text S2: Surface fields Fig. S2 displays surface fields obtained in the simulations presented in Fig. 2 of the main paper (basal heating, $V = 3.4012$, $f = 0.1$, 0.14 and 0.2) and for comparison a mobile-lid regime simulation ($V = 0$, $f = 0.04$, $H = 10$). The top panel shows the horizontal profile of the Nusselt number and the bottom panel depicts the surface RMS velocity. Green curves represent a mobile lid case, orange curves show the episodic overturn presented in Fig. 2 in the main paper, purple curves displays the RO regime also shown in Fig. 2 and the light blue curve shows a simulation in the stagnant-lid regime.

The Nusselt number profile in the mobile lid regime (green curve) displays several peaks, corresponding to the ridge locations. In the regions surrounding the ridges the Nusselt

number values are around 10-15. In the episodic regime (orange curve), peaks similar to those observed in the mobile lid regime can also be found, but they do not occur everywhere since overturn events are localized. Regions of very small Nusselt number surround the peaks, corresponding to the downwellings and diffusive regions. In the stagnant lid regime, the Nusselt number oscillates between 2 and 6, following the cell geometry. In the RO regime (purple curve) only one peak is visible. Its maximum value is comparable to those observed for ridges in other regimes, but it is narrow and the Nusselt number outside the ridge region decreases rapidly to values comparable to those obtained in the stagnant-lid regime.

The bottom panel of Fig. S2 displays the surface RMS angular velocity obtained in the same models. Velocities follow a clear hierarchy from mobile down to episodic, RO and stagnant lid. The mobile lid regime displays a juxtaposition of plate-like blocks and angular velocities in the range 30 to 1000 can be observed (green curve). The velocity structure in the episodic regime is also block-shaped, but the magnitude is smaller than in the mobile-lid regime. The dimensionless velocity obtained in the RO regime (purple curve) shows a maximum at the ridge and decreases from 40 to 2 when moving away from the ridge. No plateau can be distinguished, which shows that the deformation is not localised like in mobile-lid or episodic regimes. A large depression reaching 0.01 can be observed at the antipode of the ridge (which is also visible in Fig. 1 in the main paper). The surface angular velocity in the stagnant lid regime, represented by the light blue curve, is small everywhere (between 0.01 and 1) and reflects the geometry of the underlying convection cells.

Text S3: Strain-rate fields

Fig. S3 represents the strain-rate fields for the simulations in the RO regime displayed in Fig. 1 in the main paper. We show these fields in the supporting information for a better readability of Fig. 1.

In both cases, the strain-rate patterns are divided into internal and lithospheric regions. In the internal regions, large strain-rates can be observed in upwellings and downwelling regions (yellow colours). In the basally heated simulation, the high strain-rate areas reach down to the core-mantle boundary due to the presence of plumes. In the mixed heated simulation, the strain-rate regions displaying large values are mainly localised below the lithosphere because there is very limited basal heating and the large activation volume results in a very high viscosity in the lower mantle, preventing the downwellings from reaching the core-mantle boundary.

Despite these differences, the lithospheric strain-rate is in both cases only half as much as in the convecting domain. Outside the convection cell that contains the ridge, the strain-rate is at least 3 times smaller than in the lithosphere above the main cell. In some places, the strain-rate even drops by 3 orders of magnitude compared to average lithospheric strain-rates. Therefore, the strain-rate pattern shows that the whole lithosphere surrounding the ridge slowly deforms instead of forming localised regions that would result in resurfacing events. This is valid for viscosity contrasts as large as 9 orders of magnitude. Due to the effect of plastic yielding, the effective viscosity contrast between the internal region and lithosphere is close to 10^4-10^5, as shown in Fig. 1.

Text S4: Stationarity of the RO regime

One can wonder whether the RO regime is an equilibrium state or not. In this study, we did not see the RO regime in a stationary state, but it was observed at statistical equilibrium. This is due to the fact that we only used a single bottom Rayleigh number for all simulations. Stationary states might be expected at lower Rayleigh number.

One important thing to keep in mind is that, the RO regime is itself asymmetrical, unlike stagnant-lid or mobile-lid regimes. When a solitary ridge forms, it stretches the corresponding convection cell, due to the associated spreading velocity. *Solomatov* [2004] showed that the second invariant of the stress in the lithosphere can be considered to be linearly proportional to the cell size. Therefore, when a ridge extends its cell, one can expect subduction zones to form at the edges of the cell, where stresses become larger with time. This is the main reason why RO regimes often destabilize and episodic overturns occur. The pink region in Fig. 3, labelled "Episodic-RO", represents slightly different situations. In these cases, the ridge only is not stationary since the dominant cell extends and compresses the others. This forces one of the cells to disappear. This causes an increase of the lithospheric stress outside the dominant cell. Thus, an overturn occurs outside the dominant cell. Therefore the ridge itself does not cause subduction zones in its surrounding, but induces indirectly resurfacing events in the other cells.

However, a stable RO regime can be obtained in several situations. Movie S1 provided with this supporting information shows that ridges can stabilize when the convection degree stabilizes. In this case, there is no dominant cell, and ridges repeatedly appear at different sites. Thus, even if a ridge tends to extend its cell, it eventually disappears and another cell hosting a new ridge will push the first cell, causing it to shrink back to its

initial size. This leads to a state in which cells are successively extending and contracting. Another stable situation can be found when the convection degree is sufficiently low (in our case a degree-3). Under these circumstances, the dominant cell is more extended than the other cells, but its growth is stopped by the activity of the other cells. Finally, in the deep blue regions of Fig. 3, RO regime and stagnant lid occur alternatively. This is also a situation where ridges do not generate subduction zones although we cannot call this a ridge only at equilibrium. In such a case, it seems that the high friction coefficient does not allow for extensive ridge extension. Even in case dominant cells generate ridges, they cannot extend sufficiently to compress the other cells and decrease their number. On the contrary, the ridge generates large cold downwellings, which gather at the sides of the dominant cell (because of the depth-dependence of the viscosity). This results in slow cooling of the dominant cell. This cell then decreases in size, which allows an additional cell to form, halting the ridge activity due to the corresponding lithospheric stress reduction. A long-lasting stagnant lid regime is then established until the additional cell ceases. Larger stresses cause the formation of a new ridge, restarting the whole process.

The existence and stability of the ridge only regime is critically dependent on the convection degree of the system. RO regime at equilibrium can be reached in case the number of cells stabilizes.

Finally, Fig. S4 shows the initial temperature field used in all cases. The initial conditions might have some importance since it has been shown that the convection regime can be history-dependent. This is especially relevant close to the boundary between mobile-lid and stagnant-lid regime [*Weller and Lenardic*, 2012]. Our initial field represents a warm

situation, relevant for a young planetary body. A lithosphere of reasonable thickness is prescribed from the start, corresponding to a stagnant lid situation, but it also providing a non-negligible weight on the top boundary layer. Our initial condition favors the persistence of the stagnant lid regime, since a large number of plumes forms early on, in the low viscosity (low stress) internal region. The regime map displayed in Fig. 3 might be slightly affected by the choice of the initial temperature field, but our arguments and observations would undoubtedly hold, although some regime boundaries might be shifted. Our initial condition is consistent with early conditions of planets and satellites, expected to be hot due to gravitational energy converted during accretion and differentiation of the body and due to high radiogenic heating rates.

Figure S1: Regime maps in Cartesian geometry

Figure S2: Surface fields

Figure S3: Strain-rate fields

Figure S4: Initial temperature field

Table S1.

A large table containing the results of all simulations is provided in a separate Excel file. The table provide for each simulation: the activation volume V (column 1), the corresponding vertical viscosity contrast (column 2), the friction coefficient f (column 3), the convection regime obtained at statistical equilibrium (column 4), the heating mode (column 5) and the geometry used (column 6).

Movie S1.

The movie named MovieS1.avi presents the temperature, viscosity, strain-rate, velocity and stress fields of the simulation considering $V = 18.4207$ and $f = 0.4$ in 2D spherical annulus geometry with mixed heating. This animation shows a case in which ridges repeatedly form at preferential sites following the degree imposed by the internal activity without ever breaking the lid. Preferential sites, which could potentially host a new ridge once the active one disappears, can be seen in the stress field, but the next position of the ridge is hardly predictable.

References

Foley, B., and T. Becker (2009), Generation of plate-like behavior and mantle heterogeneity form a spherical, viscoplastic convection model, *Geoch. Geophys. Geosys.*, *10*(8), doi:10.1029/2009GC002378.

Moresi, L., and V. Solomatov (1998), Mantle convection with a brittle lithosphere: Thoughts on the global tectonic style of the Earth and Venus, *Geophys. J.*, *133*, 669–682.

Solomatov, V. S. (2004), Initiation of subduction by small-scale convection, *Journ. Geophys. Res.*, *109*, B01,412.

Stein, C., J. Schmalzl, and U. Hansen (2004), The effect of rheological parameters on plate behaviour in a self-consistent model of mantle convection, *Phys. Earth. and Plan. Int.*, *142*, 225–255.

Weller, M., and A. Lenardic (2012), Hysteresis in mantle convection: Plate tectonics systems, *Geophys. Res. Lett.*, *39*(L10202), doi:10.1029/2012GL051232.

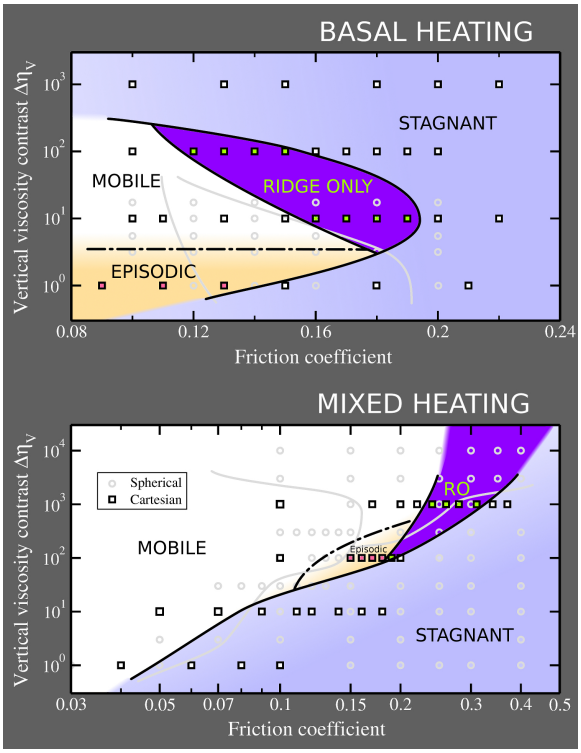

Figure 1. Maps of convection regimes in cartesian geometry for basal heating simulations (top) and mixed heating cases (bottom). See section Text S1 for a detailed description.

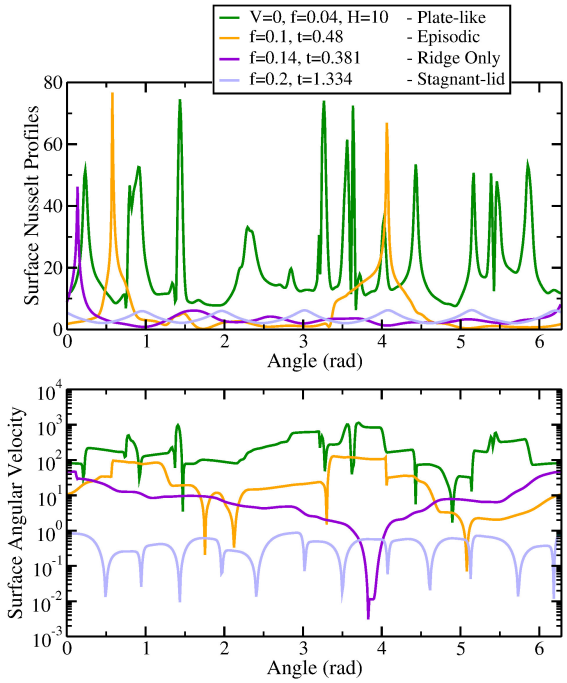

Figure 2. Surface Nusselt number profiles (top) and surface RMS angular velocities (bottom) for selected cases corresponding to the figures in the main article, considering $V = 3.4012$ and basal heating (orange, purple and blue curves) or $V = 0$ and mixed heating (green curve).

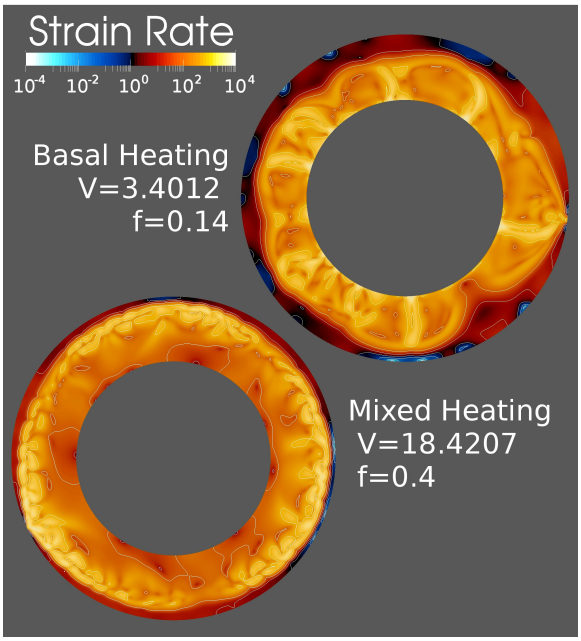

Figure 3. Second invariants of the strain-rate field in the basal heating (top) and mixed heating (bottom) simulations presented in Fig. 1 of the main article.

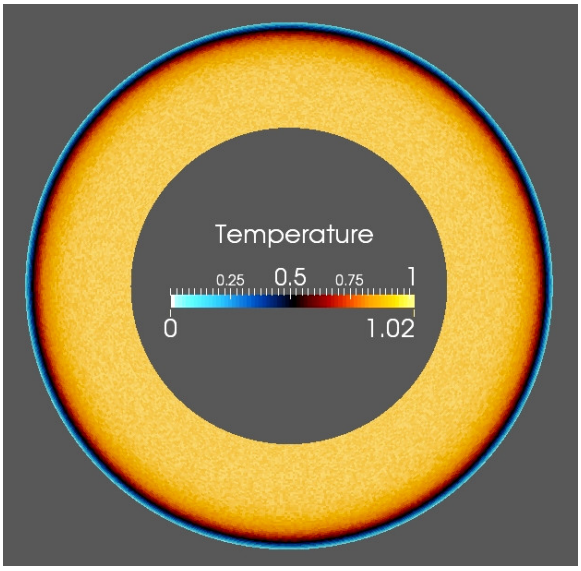

Figure 4. Initial temperature field used in all cases: a top thermal boundary layer is imposed. The internal non-dimensional temperature is set to 1. We superimpose everywhere a white noise of ± 0.25.